Mon. Not. R. Astron. Soc. **353,** 673–680 (2004) doi:10.1111/j.1365-2966.2004.08100.x

X-ray emission from a brown dwarf in the Pleiades

K. R. Briggs[1]★ and J. P. Pye[2]★

[1]*Paul Scherrer Institut, CH-5232 Villigen PSI, Switzerland*
[2]*Department of Physics and Astronomy, University of Leicester, Leicester LE1 7RH*

Accepted 2004 June 2. Received 2004 April 19

ABSTRACT

We report on the first detection of X-ray emission from a brown dwarf in the Pleiades, the M7-type Roque 14, obtained using the EPIC detectors on *XMM–Newton*. This is the first X-ray detection of a brown dwarf intermediate in age between ≈12 and ≈320 Myr. The emission appears persistent, although we cannot rule out flare-like behaviour with a decay time-scale >4 ks. The time-averaged X-ray luminosity of $L_{\rm X} \approx 3.3 \pm 0.8 \times 10^{27}$ erg s^{-1} and its ratios with the bolometric ($L_{\rm X}/L_{\rm bol} \approx 10^{-3.05}$) and H$\alpha$ ($L_{\rm X}/L_{\rm H\alpha} \approx 4.0$) luminosities suggest magnetic activity similar to that of active main-sequence M dwarfs, such as the M7 old-disc star VB 8, although the suspected binary nature of Roque 14 merits further attention. No emission is detected from four proposed later-type Pleiades brown dwarfs, with upper limits to $L_{\rm X}$ in the range 2.1–3.8 $\times 10^{27}$ erg s^{-1} and to log $(L_{\rm X}/L_{\rm bol})$ in the range −3.10 to −2.91.

Key words: stars: activity – stars: coronae – stars: individual: Roque 14 – stars: low-mass, brown dwarfs – open clusters and associations: individual: the Pleiades – X-rays: stars.

1 INTRODUCTION

Magnetic activity, generating chromospheric Hα and coronal X-ray and radio emissions, is a ubiquitous feature of main-sequence (MS) late-type stars (spectral types ≈F5–M7). Studies of these diagnostic emissions have found consistency in the character of magnetic activity throughout this range, despite the expected change in dynamo mechanism demanded by the absence of a radiative interior in stars of spectral types ≈M3 and later. However, recent studies suggest the magnetic activity of 'ultracool' objects, with spectral types ≈M8 and later, is quite different.

The observed persistent ('non-flaring') levels of X-ray ($L_{\rm X}/L_{\rm bol}$) and Hα ($L_{\rm H\alpha}/L_{\rm bol}$) emission from MS late-type stars increase with decreasing Rossby number, $Ro = P/\tau_{\rm C}$, where P is the rotation period and $\tau_{\rm C}$ is the convective turnover time, until reaching respective 'saturation' plateaus of $L_{\rm X}/L_{\rm bol} \sim 10^{-3}$ and $L_{\rm H\alpha}/L_{\rm bol} \sim 10^{-3.5}$ (e.g. Delfosse et al. 1998, for M dwarfs). The fraction of field stars showing persistent chromospheric emission levels close to saturation increases toward later spectral types, peaking around M6–7 (Gizis et al. 2000).

However, around spectral type M9 persistent Hα emission levels begin to plummet dramatically (Gizis et al. 2000). Among L-type dwarfs no rotation-activity connection is found: $L_{\rm H\alpha}/L_{\rm bol}$ continues to fall steeply toward later spectral types despite most L-dwarfs being fast rotators (Mohanty & Basri 2003). A proposed explanation is that magnetic fields diffuse with increasing efficiency in the increasingly neutral atmospheres of cooler dwarfs (Meyer & Meyer-Hofmeister 1999; Mohanty et al. 2002), overwhelming the importance of a rotation-driven dynamo efficiency in chromospheric heating. Magnetic activity is still observed, however, in the forms of Hα flaring on some L dwarfs (e.g. Liebert et al. 2003), and flaring and apparently-persistent radio emission from several ultracool dwarfs (Berger et al. 2001; Berger 2002).

Detections of X-ray emission from ultracool field dwarfs are scarce. The M7 old-disc star VB 8 shows persistent and flaring X-ray emission levels of $L_{\rm X}/L_{\rm bol} \approx 10^{-4.1}$ –$10^{-2.8}$, similar to those of active M dwarfs (Fleming et al. 1993; Schmitt, Fleming & Giampapa 1995; Fleming, Giampapa & Garza 2003). However, the persistent levels of X-ray emission from the M8 old-disc star VB 10 and the M9 ∼320-Myr-old brown dwarf LP 944-20 are at least an order of magnitude lower – $L_{\rm X}/L_{\rm bol} \approx 10^{-5.0}$ (Fleming et al. 2003) and $L_{\rm X}/L_{\rm bol} < 10^{-5.7}$ (Rutledge et al. 2000), respectively – despite the latter being a fast rotator ($v \sin i = 30$ km s^{-1}). Yet transient strong magnetic activity is evidenced by the flaring X-ray emission, with peak $L_{\rm X}/L_{\rm bol} \approx 10^{-3.7}$ –$10^{-1.0}$, that has been observed on both VB 10 (Fleming, Giampapa & Schmitt 2000) and LP 944-20, and on the M9 field dwarfs LHS 2065 (Schmitt & Liefke 2002) and 1RXS J115928.5−524717 (Hambaryan et al. 2004). Interestingly, the temperature of the dominant X-ray-emitting plasma appears to be low, $T \approx 10^{6.5}$ K, whether it is measured in the persistent (VB 10) or flaring (LP 944-20 and 1RXS J115928.5−524717) emission state. While such low temperatures are typical for the persistent coronae of inactive stars – M dwarfs (Giampapa et al. 1996) and the Sun (Orlando, Peres & Reale 2000) alike – the temperatures of flaring plasma are significantly higher, with $T > 10^{7.0}$ K (Reale, Peres & Orlando 2001; Güdel et al. 2004).

As very young substellar objects ($t \lesssim 5$ Myr) may have photospheres as warm as MS M5–6 dwarfs, an individual brown dwarf may experience a transition from 'stellar-like' to 'ultracool'

★E-mail: briggs@astro.phys.ethz.ch (KRB); pye@star.le.ac.uk (JPP)

magnetic activity as it cools. Brown dwarfs in star-forming regions are routinely observed to emit X-rays at high levels, $L_X/L_{bol} \gtrsim 10^{-3.5}$, arising from plasma at $T \gtrsim 10^{7.0}$ K, similar to those of dMe stars and higher-mass young stars (e.g. Neuhäuser & Comerón 1998; Imanishi, Tsujimoto & Koyama 2001; Feigelson et al. 2002; Mokler & Stelzer 2002; Preibisch & Zinnecker 2002). The ≈12-Myr-old, low-mass brown dwarf TWA 5B, of ultracool spectral type M8.5–9, exhibits apparently persistent X-ray emission at $L_X/L_{bol} \approx 10^{-3.4}$, like younger brown dwarfs, but with $T \approx 10^{6.5}$ K (Tsuboi et al. 2003), like field ultracool dwarfs and LP 944-20.

At around spectral type M8–9, between the ages of ∼10 and ∼300 Myr for brown dwarfs, persistent X-ray emission levels appear to fall by a factor of ∼100 and coronal temperatures appear constrained to $T \lesssim 10^{6.5}$ K, even during flares and at high emission levels. The population of brown dwarfs in the Pleiades cluster, 135 pc away (Pan, Shao & Kulkarni 2004), of age ≈125 Myr (Stauffer, Schultz, & Kirkpatrick 1998) and spanning spectral types M6.5–early-L (Martín et al. 1998), is therefore crucial to understanding the evolution of substellar magnetic activity and the conflict of a rotationally-driven magnetic dynamo against atmospheric neutrality. *ROSAT* observations of brown dwarfs in the Pleiades detected no X-ray emission at the level of $L_X/L_{bol} \gtrsim 10^{-2.5}$ (Neuhäuser et al. 1999, hereafter N99; see Section 4.4).

We present a deeper X-ray (0.3–4.5 keV) observation of five candidate brown dwarfs in the Pleiades (described in Section 2), using the more sensitive *XMM–Newton* observatory (Section 3). We detect X-ray emission from the M7 Roque 14, investigate its temporal and spectral nature, and place upper limits on the X-ray emission levels of the undetected brown dwarfs: Teide 1, Roque 9, Roque 11 and Roque 12 (Section 4). We discuss the relative X-ray and Hα emissions of these objects in the context of magnetic activity on ultracool dwarfs and its evolution (Section 5) and close by summarizing our findings (Section 6).

2 SAMPLE OF BROWN DWARFS IN THE PLEIADES

Five objects in our *XMM–Newton* field have been proposed as candidate brown dwarf members of the Pleiades on the basis of optical and near-infrared (NIR) photometry in the *IZJHK* bands (Zapatero Osorio, Rebolo & Martín 1997a; Pinfield et al. 2000, 2003). Observed and derived physical parameters are listed in Table 1. All except Roque 9 have published spectral types consistent with those expected of ≈125-Myr-old brown dwarfs. Further evidence for or against membership of the Pleiades and hence substellar status is summarized below.

Teide 1 is the on-axis target of the *XMM–Newton* observation. Its status as a brown dwarf member of the Pleiades is well established on the basis of its proper motion (Rebolo, Zapatero Osorio & Martín 1995), the detection of Li in its spectrum and its radial velocity (Rebolo et al. 1996). It shows Hα emission with variable equivalent width, $EW_{H\alpha} = 3.5$–8.6 Å (Rebolo et al. 1995, 1996). It has been suspected to have a lower-mass companion from its position on a *JK* colour–magnitude diagram (Pinfield et al. 2003).

Roque 11 has an anomolous position on a *JHK* colour–colour diagram (Pinfield et al. 2003) but its radial velocity of -3.5 ± 7 km s^{-1} is consistent with those of other Pleiades members, and its Na I absorption is lower than that of field stars of the same spectral type, indicating lower gravity, and hence youth (Zapatero Osorio et al. 1997b).

Roque 12 has a radial velocity consistent with Pleiades membership (Festin 1998), low Na I absorption and is a strong Hα emitter with $EW_{H\alpha} = 19.7$ Å (Martín et al. 1998).

Roque 14 has low Na I absorption and strong Hα emission with $EW_{H\alpha} = 17.0$ Å (Zapatero Osorio et al. 1997b). It has been suspected to be a near-equal mass binary on the basis of its position in an *IK* colour–magnitude diagram (Pinfield et al. 2003) but no comparably bright companion with separation >0.1 arcsec has been found (Martín et al. 2000).

Roque 9 has no published spectral type but we estimate a spectral type of M8 as its NIR photometry is similar to those of Teide 1 and Roque 11.

We shall use the term 'brown dwarf' to refer to all five objects, but note that the evidence in support of substellar status varies across the sample, and is weak for Roque 9.

3 OBSERVATION AND DATA ANALYSIS

The *XMM–Newton* observation, 0094780101, was centred on Teide 1 (J2000: $\alpha = 03^h47^m18\overset{s}{.}0$, $\delta = +24^\circ22'31''$) and conducted on 2000 September 1 in orbit 134. The thick optical blocking filter was placed in front of all three EPIC detectors: the pn (Strüder et al. 2001) was exposed for 40.6 ks and each MOS (M1 and M2; Turner et al. 2001) for 33.0 ks, beginning 7.5 ks later. The data were processed using the SCIENCE ANALYSIS SYSTEM (SAS) v5.4.1 [1] and each EPIC event list was further filtered to exclude flagged 'bad' events, and uncalibrated event patterns (>12 for MOS; >4 for pn). Several short intervals affected by high background were also excluded. We considered only events with PI in the range 300–4500 (nominally energies of 0.3–4.5 keV, and PI is reported in units of eV or keV from this point) to reduce background contamination.

We extracted an image with 4×4 arcsec^2 pixels from each detector and performed source detection in each image. The procedure, using tasks available in SAS, is described in detail in Briggs & Pye (in preparation). In brief, potential sources were located using a wavelet detection package (EWAVELET), and masked out of the photon image while it was adaptively smoothed (using ASMOOTH) to generate a model of the background. The spatial variation of vignetting and quantum efficiency was modelled in an exposure map (produced using EEXPMAP). The images, background and exposure maps [2] of the three EPIC instruments were also mosaicked to optimize the sensitivity of the analysis and EWAVELET was used to locate potential sources in the EPIC image. In each image, at the position of each EWAVELET source, a maximum likelihood fitting of the position-dependent instrument point spread function (PSF) was applied (EMLDETECT) to parametrize each source and those with $ML > 6$ were retained. EMLDETECT additionally reconstructed a smooth model of the input image by adding PSFs to the background map with the location, normalization and extent of the parametrized sources. We repeated the source detection procedure on 20 images generated from this model image using Poisson statistics, and 20 images generated from the source-free background map. We found in both cases a mean number of false detections per image of five with $ML > 6$ and two with $ML > 7$.

Approximately 130 X-ray sources were found, of which 34 were associated with proposed members of the Pleiades. Matching of the

[1] See http://xmm.vilspa.esa.es/.

[2] The pn exposure map must be scaled by a factor to account for its higher sensitivity compared to M1 and M2. This factor is dependent on the source spectrum and discussed in Section 4.3.

Table 1. Observed and derived physical parameters of the studied brown dwarfs. The columns show the following: (1)–(3) name and alternative designations; (4) and (5) RA and Dec. (J2000; Pinfield et al. 2000); (6)–(8) *J*, *H* and *K* magnitudes (Pinfield et al. 2000; 1σ uncertainties are $\leqslant$0.05 mag); (9) spectral type; (10) reference for spectroscopy – Rebolo et al. 1995 (R95), Zapatero Osorio et al. 1997b (Z97), 1999 (Z99), Martín et al. 1998 (M98); (11) effective temperature in K (assigned from spectral type after Mohanty & Basri 2003); (12) and (13) mass ($M_\odot$) and bolometric luminosity (10^{30} erg s^{-1}) calculated from $T_{\rm eff}$ using models of Baraffe et al. (1998) for age 125 Myr; (14) binary mass ratio where binarity is indicated (Pinfield et al. 2003).

Name (1)	BPL (2)	NPL (3)	RA (4)	Dec. (5)	*J* (6)	*H* (7)	*K* (8)	SpT (9)	Ref (10)	$T_{\rm eff}$ (11)	$M_\star$ (12)	$L_{\rm bol}$ (13)	*q* (14)
Roque 14	108		$03^{\rm h}46^{\rm m}42\overset{\rm s}{.}90$	$+24^\circ24'50\overset{''}{.}4$	15.50	14.89	14.47	M7.0	Z97	2700	0.066	3.7	0.75–1
Roque 12	172	36	$03^{\rm h}48^{\rm m}18\overset{\rm s}{.}96$	$+24^\circ25'12\overset{''}{.}9$	15.91	15.36	15.10	M7.5	M98	2625	0.061	3.1	
Teide 1	137	39	$03^{\rm h}47^{\rm m}17\overset{\rm s}{.}83$	$+24^\circ22'31\overset{''}{.}5$	16.32	15.62	15.08	M8.0	R95	2550	0.056	2.7	0.5–0.9
Roque 11	132	37	$03^{\rm h}47^{\rm m}12\overset{\rm s}{.}02$	$+24^\circ28'31\overset{''}{.}5$	16.03	15.64	15.13	M8.0	Z99	2550	0.056	2.7	
Roque 9	100		$03^{\rm h}46^{\rm m}23\overset{\rm s}{.}05$	$+24^\circ20'36\overset{''}{.}1$	16.28	15.63	15.22	(M8.0)		(2550)	(0.056)	(2.7)	

EMLDETECT source positions with NIR positions of these members (Pinfield et al. 2000) revealed a boresight shift in the EPIC image of $\alpha_{\rm X}\cos\delta_{\rm X} - \alpha_{\rm NIR}\cos\delta_{\rm NIR} = 3.7$ arcsec and $\delta_{\rm X} - \delta_{\rm NIR} = -0.8$ arcsec, which is accounted for in the remainder of this work. The corrected positions of sources associated with the Pleiades were all within 6 arcsec of the NIR positions. The probabilities of a positional coincidence within 6 arcsec of a brown dwarf with a spurious detection or a source unrelated to the Pleiades are $\approx 10^{-3}$ and $\approx$0.02, respectively.

ML-fitting was performed in each image at the NIR position of each brown dwarf. The successful detection of Roque 14 is described further in Section 4.1, and investigations of the temporal and spectral nature of its emission are pursued in Sections 4.2 and 4.3, respectively. In no other case was an *ML* value >1 found. Upper limits to the X-ray luminosity of these objects are calculated in Section 4.4.

4 RESULTS

4.1 An X-ray detection of Roque 14

Roque 14 was returned as an X-ray source by EWAVELET in the M2, pn, and mosaicked-EPIC images. EMLDETECT determined *ML* values of 2.1, 5.9 and 7.0 (1.6, 3.0 and 3.3 σ) in these respective images, confirming the detection at *ML* >6 (3.0 σ) only in the mosaicked-EPIC image [3] (Fig. 1a). The best-fitting X-ray source position in the EPIC image was 0.8 arcsec offset from the NIR position. We estimated the 1σ uncertainty in the relative positions as the sum in quadrature of the statistical fitting uncertainty, 0.73 arcsec, an uncertainty in the EPIC absolute pointing of 1.0 arcsec, and an uncertainty in the optical position of 0.5 arcsec; thus the positional offset of the source is $\approx$0.6 σ. The total number of EPIC source counts determined by EMLDETECT was 24.7 $\pm$ 5.9. We calculate the X-ray luminosity after consideration of the source spectrum in Section 4.3.

Further analysis of the X-ray emission from Roque 14 has been conducted both including and excluding periods affected by high background, and no significant improvement has been found by excluding those periods. Therefore, to maximize the number of events available, we report on the results of including the short periods of high background.

We extracted source events from a circle centred on the best-fitting source position with radius 10.75 arcsec, which encloses only 54 per cent of the source counts (Ghizzardi 2002) but optimizes the signal-to-noise ratio, and background events from the surrounding annulus, eight times larger than the source extraction region. M1 and M2 event lists were combined as these instruments have near-identical sensitivity, spectral response and exposure length. A total of 32 counts in all EPIC instruments (23 from pn and nine from the two MOS cameras) was extracted from the source region and 140 (99 pn; 41 MOS) counts from the background region. Thus we expect 17.5 (12.4 pn; 5.1 MOS) background counts in the source region. As the background region will contain $\approx$46 per cent of the $\approx$25 source counts, we expect a contribution of source counts ($\approx$1.4) similar to the 1σ uncertainty ($\approx$1.2) in the estimated mean background counts. The probability of 32 counts or more appearing in the source region as a result of a Poissonian fluctuation in a mean background of 17.5 counts is 0.0011 (3.2 σ), in support of the EMLDETECT detection.

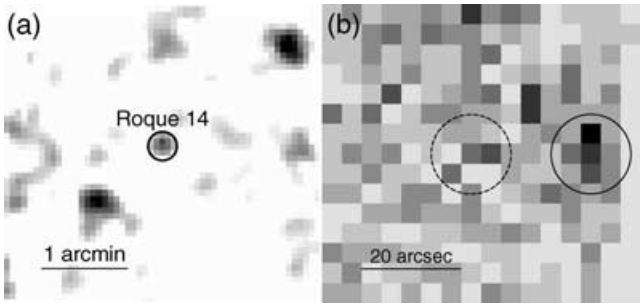

Figure 1. (a) Adaptively smoothed EPIC 0.3–4.5 keV image of the region around Roque 14. The circle is centred on the NIR position. (b) Mosaicked EPIC 0.3–1.4 keV image of a composite of the four undetected brown dwarfs. The dotted circle of 8-arcsec radius centred on the NIR position marks the region used to estimate upper limits. The circled source 25 arcsec to the west is not associated with the Pleiades.

The events extracted from the source region were used to examine the temporal and spectral behaviour of Roque 14. Events were extracted from a larger source-free region on the same CCD as Roque 14 to make a better model of the time and energy distribution of the background.

4.2 Transient or persistent emission?

Examination of the arrival times of the photons in the source event list suggests a concentration, particularly of lower-energy (0.3–1.4 keV) events, in the $\approx$10-ks interval 10–20 ks after the start of the pn exposure (Fig. 2).

We investigated the statistical significance of this possible variability using the Kolmogorov–Smirnov (K–S) statistic. The K–S

[3] *ML* values output by EMLDETECT have been corrected as advised in *XMM News 29*.

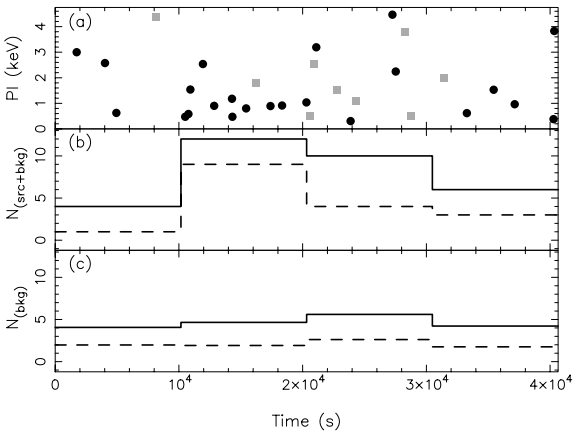

Figure 2. (a) The arrival time and energy of each pn (black circles) and MOS (grey squares) event detected in the Roque 14 source extraction region. In (b) the observation has been divided into four equal time intervals to bin all the events. (c) shows the expected contribution of background events. The bold and dashed histograms are for events in the 0.3–4.5 and 0.3–1.4 keV energy bands, respectively. There is an apparent concentration of 0.3–1.4 keV events in the second interval.

statistic is the maximum vertical difference between the cumulative distribution functions (CDFs) of an observed data set and a test distribution (or two observed data sets). As our test model must account for the significant number of background events in the source extraction region, which is subject to Poissonian fluctuations about its expected number, we have performed Monte Carlo simulations to assess the confidence level of deviation from the test model as a function of K–S value.

Our test-model CDF was constructed from the arrival times of events in the background extraction region and arrival times of a number of source events (such that the ratio of source-to-background counts was as estimated from the observed data) chosen at uniform intervals in the CDF of a constant count-rate source. Sets of arrival times for pn and MOS events were constructed separately and then merged before calculating the test-model CDF for all EPIC data (Fig. 3a).

Each trial data set in our simulations was composed of the observed numbers of pn (23) and MOS (9) events. The number of background events was drawn from a Poisson distribution with mean value as estimated from the data. Arrival times for these background events were drawn at random from the observed distribution for background events. Arrival times for the remaining events were drawn at random from the modelled distribution for source events. MOS and pn data sets were again constructed separately before being combined. For each trial data set the K–S statistic was calculated. The CDF of these K–S values gives the confidence level of deviation from the test model as a function of measured K–S value (Fig. 4a).

The simulated distribution of K–S values for a test model of a constant source count-rate, based on 10 000 trials, is practically indistinguishable from the standard calculated distribution. The K–S value of the observed data set for this test model is 0.110 (Fig. 3c), which corresponds to just 20 per cent confidence that the source count rate is not constant. Following the same procedure, we have additionally tested models in which the source emission is purely transient (Fig. 3a), with the profile of fast (here, instantaneous) rise and exponential decay typical of flares on late-type stars, beginning 10 ks after the start of the pn observation. For short decay time-

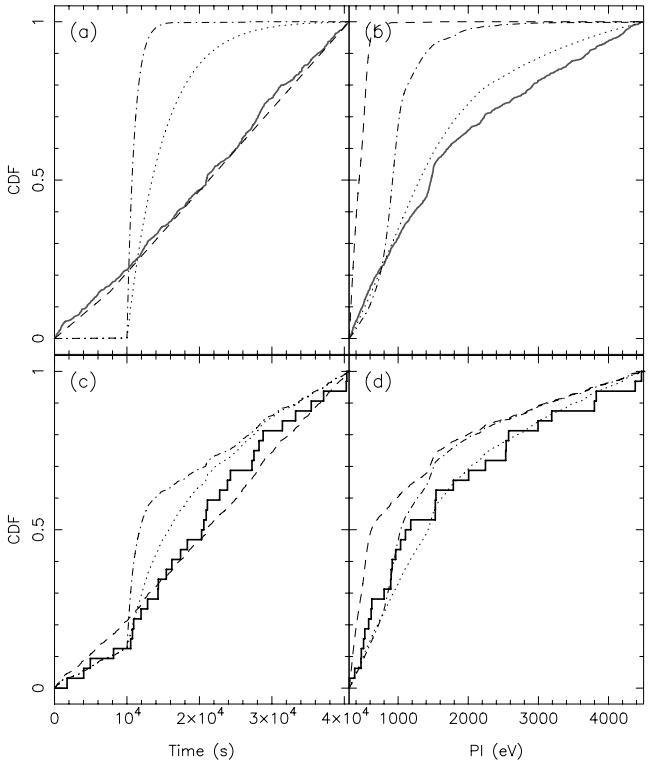

Figure 3. Cumulative distribution functions of event arrival times (a and c) and PI values (b and d). Bold lines are for observed background (grey in a and b) and source+background (black in c and d) data. Broken lines are for modelled source (a and b) and source+background (c and d) data. In (a) and (c) the dashed line is for a constant source count rate, while dot-dashed and dotted lines assume all source counts arise from a flare with exponential decay on respective time-scales of 1000 and 5000 s. In (b) and (d) the dashed, dot-dashed, and dotted lines are for source temperatures of $10^{6.0}$, $10^{7.0}$ and $10^{8.0}$ K, respectively. A K–S test rules out the temporal model of a flare with decay time-scale 1000 s and the $10^{6.0}$ K spectral model at 90 per cent confidence.

scales, when the source and background models are starkly different (Fig. 3a), Fig. 4a shows that the standard calculation significantly overestimates the simulated confidence level of deviation from the test model. The K–S test rules out flare models with decay time-scale of 3 ks or less at the 90 per cent confidence level, but permits those with time-scale 4 ks or longer (Fig. 3c).

We therefore cannot exclude the possibility that the observed emission from Roque 14 was due to a flare-like outburst similar to those with decay time-scales of ∼5 ks seen from the M9 ultracool dwarfs LP 944-20 (Rutledge et al. 2000), LHS 2065 (Schmitt & Liefke 2002), and RXS J115928.5-524717 (Hambaryan et al. 2004).

4.3 Temperature of X-ray emitting plasma

Fig. 2 suggests the excess of counts was chiefly in the low-energy (0.3–1.4 keV) band, indicative of plasma with temperature $T \lesssim 10^{7.25}$ K typical in coronae on late-type stars.

We attempted to constrain the source temperature by implementing a K–S test of the PI values of the observed events, as described above for arrival times. Model distributions of PI values were tested for an isothermal optically-thin plasma source, with an array of temperatures, T, at intervals of 0.25 dex in log T in the range $6.0 \leqslant \log T \leqslant 8.0$ K (Fig. 3b). Each source model was generated in XSPEC (Arnaud 1996) using an APEC model (Smith et al. 2001) with solar abundances and absorbing column density typical for the Pleiades,

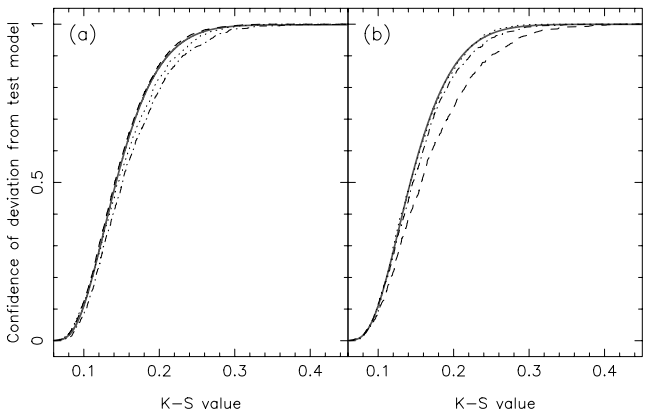

Figure 4. Confidence level of deviation from the test model as a function of K–S test value resulting from Monte Carlo simulations of (a) arrival time and (b) PI of 32 pn and MOS source and background events (see text for more details). The line styles of black lines represent the same source models as in Fig. 3. Solid lines show the standard calculated relation. When source and background distributions differ appreciably, the calculated confidence may significantly overestimate the true confidence.

$N_{\rm H} = 2.0 \times 10^{20}$ cm^{-2} (Paresce 1984; Stauffer 1984), convolved with the pn response matrix and ancilliary response at the source position.

While it was possible to rule out models with $T < 10^{6.5}$ K at the 90 per cent confidence level, due to the small number of counts and the hard spectrum of the significant number of background events we were unable to exclude high source temperatures, even up to $10^{8.0}$ K (Fig. 3d).

For a plasma temperature of $10^{7.0}$ K, the sensitivity ratio of pn to MOS is 3.6 in the 0.3–4.5 keV energy band and the MOS count-to-flux conversion factor is 6.4×10^{-12} erg cm^{-2} s^{-1} per (0.3–4.5 keV) count s^{-1}. Thus, the total MOS-equivalent effective exposure time for Roque 14 was 117.6 ks, its MOS-equivalent count-rate was $2.1 \pm 0.5 \times 10^{-4}$ count s^{-1}, and its time-averaged X-ray luminosity was $3.3 \pm 0.8 \times 10^{27}$ erg s^{-1}, with $L_{\rm X}/L_{\rm bol} \approx 10^{-3.05}$. The assumption of a plasma temperature of $10^{6.5}$ K would give $L_{\rm X} \approx 3.5 \pm 0.8 \times 10^{27}$ erg s^{-1}.

4.4 Upper limits to X-ray emission from undetected brown dwarfs

No significant X-ray emission was detected from any of the remaining four brown dwarfs. [4] At the NIR position of each brown dwarf, we counted events detected by each EPIC instrument in the 0.3–1.4 keV energy range.[5] A radius of 8 arcsec was used to minimize counts from nearby sources to Roque 11 and Teide 1. The expected number of background counts was estimated from the value at the source position in the reconstructed image generated by EMLDETECT in the 0.3–1.4 keV band. This enabled us to account for stray counts from nearby sources, and we note that the respective backgrounds for Teide 1 and Roque 11 were thus 25 and 36 per cent higher than the values at those positions in the ASMOOTH background map. Upper limits to the source counts at 95 per cent confidence were calculated using the Bayesian method described by Kraft, Burrows & Nousek (1991).

These upper limits were corrected for the enclosed energy fraction at the source off-axis angle (0.40–0.46 for a radius of 8 arcsec; Ghizzardi 2002) and converted to MOS-equivalent count rates by dividing by the value at the source position in the MOS-equivalent EPIC exposure map. The assumption of a $10^{7.0}$ K plasma with solar abundances and $N_{\rm H} = 2 \times 10^{20}$ cm^{-2} gives a MOS count-to-flux conversion factor of 7.2×10^{-12} erg cm^{-2} s^{-1} per (0.3–1.4 keV) count s^{-1} and upper limits to the 0.3–4.5 keV X-ray luminosity in the range 1.9 –3.4 $\times 10^{27}$ erg s^{-1}, with upper limits to $L_{\rm X}/L_{\rm bol}$ in the range $10^{-3.10}$ –$10^{-2.91}$ (listed in Table 2).

To optimize our sensitivity to the detection of X-ray emission from these brown dwarfs and to put the tightest possible constraint on their mean X-ray luminosity, we constructed a composite image of all the available EPIC data in 1 × 1 arcmin^2 squares centred on the NIR positions of the four brown dwarfs (Fig. 1b). The total MOS-equivalent exposure time for the composite brown dwarf was 439.3 ks. EMLDETECT detected the source ≈25 arcsec west of Roque 11, but no source at the position of the composite brown dwarf. We calculated an upper limit to the mean X-ray luminosity of the four brown dwarfs of 1.1×10^{27} erg s^{-1} using the method described above. This corresponds to a mean $L_{\rm X}/L_{\rm bol}$ of $10^{-3.4}$. Deeper observations or a composite analysis of a larger sample are required to determine if the mean activity level of Pleiades brown dwarfs lies well below the saturated level.

Considerably lower 2σ (≈95 per cent confidence) upper limits, to $L_{\rm X}$ in the range 5.2 –9.5 $\times 10^{26}$ erg s^{-1}, and to $L_{\rm X}/L_{\rm bol}$ in the range $10^{-3.83}$ –$10^{-3.43}$, have been reported for these objects (excepting Roque 9) by N99 using a number of observations of the Pleiades by the *ROSAT* Position Sensitive Proportional Counter (PSPC). All five brown dwarfs were included in seven separate exposures longer than 1.5 ks of four different PSPC pointings in the *ROSAT* public archive; the total exposure time of each field ranged from 22.5–39.9 ks. They were best observed in the 'Pleiades Centre' field, at off-axis angles in the range 14–24 arcmin. The longest of the three exposures of this field, 22.4 ks from a total of 35.4 ks, was not used in N99, probably due to a faulty aspect solution (Hodgkin, Jameson & Steele 1995). We have recalculated 95 per cent confidence upper limits by applying the Bayesian method as described above, using the broad-band (0.1–2.4 keV) images, background maps and exposure maps of the six remaining archival exposures, and merging data from exposures of the same field. We used a variety of extraction radii in each field and further combined data from different fields obtained with similar enclosed energy fraction (calculated using Boese 2000, equation 9), to find the strictest upper limit for each brown dwarf. We were also mindful of avoiding nearby X-ray sources detected by *XMM–Newton*. Optimum enclosed energy fractions ranged from 0.35–0.75. We converted PSPC count rates to unabsorbed fluxes in the 0.1–2.4 keV band using a conversion factor of 1.0×10^{-11} erg cm^{-2} s^{-1} per count s^{-1}, appropriate for a $10^{7.0}$ K plasma with low absorption, as used in N99. Fluxes in the 0.3–4.5 keV energy band would be 5 per cent higher. A distance of 135 pc was used to calculate luminosities (N99 used 125 pc).

[4] A source detected by a previous analysis 15 arcsec from Roque 9 only in the 0.8–1.5 keV band is not recovered in this procedure, and was in any case considered more likely to be the chance alignment of a background source (Briggs & Pye 2003b).

[5] For a $T = 10^{7.0}$ K plasma with solar abundances and $N_{\rm H} = 2 \times 10^{20}$ cm^{-2} the 0.3–1.4 keV energy band enables detection at a given signal-to-noise ratio against the observed background spectrum for the lowest total of 0.3–4.5 keV source counts. The required number of source counts is only slowly increasing with the upper energy bound up to 4.5 keV and we do not find better constraint of the Roque 14 source variability or plasma temperature using this stricter energy cut.

Table 2. X-ray and Hα properties of the studied brown dwarfs. The columns show the following: (2) total MOS-equivalent effective exposure time in s; (3) number of EPIC source counts and 1σ uncertainty, or 95 per cent upper limit; (4) MOS-equivalent count rate (10^{-4} s^{-1}) and 1σ uncertainty, or 95 per cent upper limit; (5) X-ray luminosity in 10^{27} erg s^{-1} in the 0.3–4.5 keV band and 1σ uncertainty, or 95 per cent upper limit; (6) logarithmic ratio of X-ray and bolometric luminosities; (7) equivalent width of Hα (Å); (8) logarithmic ratio of Hα and bolometric luminosities (calculated as in Mohanty & Basri 2003); (9) ratio of X-ray and Hα luminosities.

Name (1)	$T_{\rm exp}$ (2)	$N_{\rm X}$ (3)	$C_{\rm X}$ (4)	$L_{\rm X}$ (5)	log $(L_{\rm X}/L_{\rm bol})$ (6)	EW$_{\rm H\alpha}$ (7)	log $(L_{\rm H\alpha}/L_{\rm bol})$ (8)	$L_{\rm X}/L_{\rm H\alpha}$ (9)
Roque 14	117 590	24.7 ± 5.9	2.1 ± 0.5	3.3 ± 0.8	-3.05	17.0	-3.66	4.0
Roque 12	26 300	< 6.5	< 2.48	< 3.8	< -2.91	19.7	-3.69	<6
Teide 1	194 250	<26.9	< 1.39	< 2.1	< -3.10	3.5,8.6	-4.53,-4.14	<27,<11
Roque 11	145 080	<21.1	< 1.46	< 2.3	< -3.08	5.8	-4.31	<17
Roque 9	73 640	<11.6	< 1.57	< 2.5	< -3.04			

Table 3. X-ray and Hα properties of ultracool field dwarfs. The columns show the following: (2) spectral type; (3) bolometric luminosity in 10^{30} erg s^{-1} (as published for VB 8, VB 10 and LP 944-20; as calculated from Baraffe et al. 1998 for age $> 10^9$ yr and $T_{\rm eff} = 2475$ K for LHS 2065); (4) emission type (flaring, F, or non-flaring, N); (5) logarithmic ratio of X-ray and bolometric luminosities; (6) reference for X-ray emission; (7) equivalent width in Hα in Å; (8) logarithmic ratio of Hα and bolometric luminosities (calculated as in Mohanty & Basri 2003); (9) reference for Hα emission; (10) ratio of X-ray and Hα luminosities.

Name (1)	SpT (2)	$L_{\rm bol}$ (3)	Em (4)	log $(L_{\rm X}/L_{\rm bol})$ (5)	Ref$_{\rm X}$ (6)	EW$_{\rm H\alpha}$ (7)	log $(L_{\rm H\alpha}/L_{\rm bol})$ (8)	Ref$_{\rm H\alpha}$ (9)	$L_{\rm X}/L_{\rm H\alpha}$ (10)
VB 8	M7.0	2.40	F	-2.8	Schmitt et al. (1995)	20.4	-3.58	Tinney & Reid (1998)	6.0
			N	-3.5	Fleming et al. (1993)	6.8	-4.06	Mohanty & Basri (2003)	3.6
			N	-4.1	Fleming et al. (2003)	3.7	-4.32	Tinney & Reid (1998)	1.7
VB 10	M8.0	1.70	F	>-2.8	Fleming et al. (2000)				
			N	-4.9	Fleming et al. (2003)	5.6	-4.32	Mohanty & Basri (2003)	0.3
			N	<-5.0	Fleming et al. (2000)	4.1	-4.46	Martín (1999)	<0.3
LHS 2065	M9.0	1.20	F	-2.5	Schmitt & Liefke (2002)	261.0	-2.84	Martín & Ardila (2001)	2.2
			N	$\lesssim -3.7$	Schmitt & Liefke (2002)	9.0	-4.30	Mohanty & Basri (2003)	$\lesssim 4.0$
			N	<-3.8	Schmitt & Liefke (2002)	7.5	-4.38	Martín & Ardila (2001)	<3.8
LP 944-20	M9.0	0.57	F	-3.7	Rutledge et al. (2000)				
			N	<-5.7	Rutledge et al. (2000)	1.0	-5.26	Mohanty & Basri (2003)	<0.4

The tightest upper limits to the X-ray luminosity we could apply were 1.2 –2.5 $\times$ 10^{28} erg s^{-1} for Roque 9, 14, 11, and 12, and 4.3 $\times$ 10^{28} erg s^{-1} for Teide 1, which may be contaminated by stray counts from the X-ray-bright K5 Pleiad HII 1348, $\approx$50 arcsec away (Briggs & Pye 2003a). Upper limits to $L_{\rm X}/L_{\rm bol}$ were in the range $10^{-2.4}$ –$10^{-1.8}$. Hence, we conclude that the *ROSAT* observations were not sufficient to detect Roque 14 at the level detected here by *XMM–Newton*, and the current *XMM–Newton* observation places the strictest upper limits thus far to the X-ray emission levels of Pleiades brown dwarfs of spectral type M7.5–8.

5 DISCUSSION

5.1 X-ray emission from ultracool dwarfs

We have detected X-ray emission only from the M7-type Roque 14 at $L_{\rm X}/L_{\rm bol} \approx 10^{-3.05}$, and placed an upper limit to the mean emission level from the four later-type Pleiades brown dwarfs at $L_{\rm X}/L_{\rm bol} < 10^{-3.4}$. This is consistent both with the pattern of emission from active MS M stars, which scales with bolometric luminosity, and with the idea that persistent X-ray emission levels fall around spectral type M8 as magnetic field dissipates more easily in cooler, more neutral lower atmospheres.

We can make some comparison of the character of the magnetic activity of Roque 14 with that of other low-mass stars based on the relative levels of chromospheric and coronal emission. Fleming (1988) has reported a mean ratio of $L_{\rm X}/L_{\rm H\alpha} \approx 6.7$ for a sample of the active, frequently-flaring, dMe stars and Reid, Hawley & Mateo (1995) have reported a value of $\sim$3 for M0–6 field stars outside flares. Unfortunately, $L_{\rm H\alpha}$ and $L_{\rm X}$ are both typically variable and simultaneous measurements are scarce. Observed values and calculated ratios of $L_{\rm X}$ and $L_{\rm H\alpha}$ for the Hα- and X-ray-detected dwarfs VB 8, VB 10, LHS 2065 and LP 944-20 are listed in Table 3. We stress that these $L_{\rm X}/L_{\rm H\alpha}$ ratios are not calculated from simultaneous measurements of $L_{\rm X}$ and $L_{\rm H\alpha}$, but from a simple ranking of the observed values of each. Nevertheless, a striking change in non-flaring emission appears to take place between the M7 star VB 8, in which $L_{\rm X} > L_{\rm H\alpha}$ and the M8 and M9 dwarfs VB 10 and LP 944-20, in which $L_{\rm X} < L_{\rm H\alpha}$ (noted by Fleming et al. 2003). This suggests that the efficiency of persistent coronal heating decays more quickly in response to the increasingly neutral atmosphere of ultracool dwarfs than the efficiency of chromospheric heating. Within the same sample, excluding LP 944-20, transition region heating, inferred from C IV emission, appears to remain as efficient as chromospheric heating (Hawley & Johns-Krull 2003).

The ratio of the single measurements of $L_{\rm X}$ and $L_{\rm H\alpha}$ from Roque 14 is 4.0. If Roque 14's measured chromospheric and coronal emissions are interpreted as persistent, this suggests that its magnetic activity is of similar character to that of VB 8 and active MS M dwarfs. Although we cannot exclude that Roque 14's observed X-ray emission is solely the result of a flare with decay time-scale

∼5 ks, like the observed high-level X-ray emission from M8 old-disc star VB 10 and M9 dwarfs LP 944-20, LHS 2065 and RXS J115928.5-524717, the high Hα emission level of Roque 14 supports a persistently higher level of magnetic activity than on these cooler dwarfs.

Roque 14 has been suspected to be a near-equal-mass binary, but $L_X/L_{H\alpha} > 2$ even if the X-ray emission is interpreted as coming from two stars. [6] An observation by the *Hubble Space Telescope* NICMOS camera does not support Roque 14's binarity, finding no companion of comparable brightness at separations >0.1 arcsec, or 13.5 au (Martín et al. 2000). While interaction between two close binary components could be influential in the X-ray production mechanism, the emission is at a similar level to that produced by magnetic activity on single active MS M dwarfs.

The observed strong Hα emission from the M7.5 Roque 12 hints at activity similar to that of Roque 14. In contrast, the measured Hα emission levels of the M8 Pleiades brown dwarfs Teide 1 and Roque 11 are very like that of the M8 VB 10, and we speculate that the magnetic activity of these objects is already in the regime where $L_X < L_{H\alpha}$ and their persistent X-ray emission levels are more than an order of magnitude lower than that of Roque 14. Deeper X-ray observations are required to test this prediction.

5.2 Evolution of X-ray emission from brown dwarfs

Very young brown dwarfs in star-forming regions are now routinely observed to emit X-rays at levels of $L_X/L_{bol} \sim 10^{-4}$ –10^{-3} that arise from hot ($T > 10^7$ K) plasma (e.g. Imanishi et al. 2001; Feigelson et al. 2002; Preibisch & Zinnecker 2002). A growing body of evidence indicates that young brown dwarfs experience accretion and outflows just like young low-mass stars (Jayawardhana, Mohanty & Basri 2003). Their X-ray emission is very likely to be produced by similar means to T Tauri stars. This is probably largely coronal emission as a result of magnetic activity, as in older low-mass stars, and as young substellar objects may have photospheres as warm as 2900 K (e.g. Baraffe et al. 1998), their atmospheric conditions are ripe for the efficient coronal heating seen on active MS M5–6 stars. However, Hα emission may arise predominantly from material accreting on to the young brown dwarf, rather than from a hot chromosphere. X-ray emission levels appear to rise with Hα emission levels up to $EW_{H\alpha} \approx 20$ Å, as would be expected for Hα emission predominantly from a magnetically-powered chromosphere, but there is no detection of X-rays from a young brown dwarf with $EW_{H\alpha} > 30$ Å (Tsuboi et al. 2003). This is consistent with the scenario emerging from X-ray surveys of T Tauri stars wherein samples of stars showing signs of strong accretion, such as high $EW_{H\alpha}$, appear to show lower levels of X-ray emission than weakly-accreting objects of similar mass (e.g. Flaccomio, Micela & Sciortino 2003).

X-ray emission has been previously detected from just two brown dwarfs older than 5 Myr. While any accretion is expected to have ceased by the age of the 12-Myr-old TWA 5B, this object has a much lower mass than Roque 14, 0.014–0.043 $M_\odot$ (Neuhäuser et al. 2000), and is unlikely to be a good model for its youthful X-ray activity. Conversely, LP 944-20 appears to have a similar mass to Roque 14, 0.056 –0.064 $M_\odot$ (Tinney 1998). It has cooled to a spectral type of M9, so its lower atmosphere is highly neutral, which is probably the key reason why its persistent X-ray emission level is ∼100 times lower than those of many very young brown dwarfs and the detected level from Roque 14. However, we should be wary of assuming that the activity levels of all coeval brown dwarfs are the same, and that Roque 14 and LP 944-20 are representative of their respective ages. There is a large spread in the observed L_X/L_{bol} values of young brown dwarfs, a significant number being undetected at upper limits $<10^{-4}$ (e.g. Imanishi et al. 2001). Roque 14 has one of the highest Hα emission levels among Pleiades brown dwarf candidates (Zapatero Osorio et al. 1997b), while LP 944-20 has one of the lowest among M9 field dwarfs (Mohanty & Basri 2003). So, while we may expect the X-ray emission level of brown dwarfs to decrease as they age from ≈125 to ≈320 Myr, as apparently observed by comparing Roque 14 and LP 944-20, the effect is probably exaggerated in choosing these two objects as representative. Larger, and necessarily deeper, surveys of the X-ray emission of brown dwarfs in the field and in the Pleiades (and other clusters) are required to make further progress in understanding the evolution of the magnetic activity of substellar and ultracool objects.

[6] As $L_{H\alpha}/L_{bol}$ is calculated here from $EW_{H\alpha}$, as a ratio with the continuum, it should be little changed whether there is one source or are two similar sources.

6 SUMMARY

We have observed five candidate brown dwarfs in the Pleiades with *XMM–Newton*, detecting X-ray emission from the M7 Roque 14. The low number of counts and significant contribution of background counts prevent meaningful constraint of the temperature and exclusion of transient emission. Assuming a plasma temperature of $10^{7.0}$ K and nominal absorbing column to the Pleiades of 2×10^{20} cm^{-2}, the time-averaged X-ray luminosity of $L_X = 3.3 \pm 0.8 \times 10^{27}$ erg s^{-1}, and its ratios with the bolometric ($L_X/L_{bol} \approx 10^{-3.05}$) and H$\alpha$ ($L_X/L_{H\alpha} \approx 4.0$) luminosities resemble those of active MS M dwarfs, as have been observed on the M7 old-disc star VB 8.

We have placed the tightest upper limits thus far on the X-ray emission levels of the four later-type Pleiades brown dwarfs: $L_X < 2.1$–3.8×10^{27} erg s^{-1} and $L_X/L_{bol} < 10^{-3.10}$ –$10^{-2.91}$.

The *XMM–Newton* data do not exclude the fact that Roque 14's observed high level of X-ray emission is solely the result of a flare with decay time-scale ∼5 ks like the observed high-level emission from M8–9 field dwarfs VB 10, LP 944-20, LHS 2065 and RXS J115928.5-524717, but the high Hα emission level of Roque 14 is supportive of a persistently higher level of magnetic activity than on these cooler dwarfs. However, the similarity of the low Hα emission levels of Teide 1 and Roque 11 to that of the M8 old-disc star VB 10 prompts us to speculate that the persistent X-ray emission levels of M8 brown dwarfs in the Pleiades may be low, with $L_X/L_{bol} \lesssim 10^{-5}$, like those of VB 10 and the M9, ≈320-Myr-old brown dwarf LP 944-20.

Deeper X-ray observations, less contaminated by background, are required to confirm a persistent high level of X-ray emission from Roque 14, to assess its coronal temperature, and to probe the typical X-ray emission levels of Pleiades brown dwarfs. Coordinated programmes to study X-ray, Hα and radio emission from ultracool and brown dwarfs of a range of ages are required to enable significant progress toward understanding the mechanisms and evolution of magnetic activity on these low-mass, cool objects.

ACKNOWLEDGMENTS

JPP acknowledges the financial support of the UK Particle Physics and Astronomy Research Council (PPARC). The authors thank David Burrows for providing source code for calculating upper limits, and Manuel Güdel for useful discussions. This work uses data

obtained by *XMM–Newton*, a European Space Agency (ESA) science mission with instruments and contributions directly funded by ESA Member States and the USA (NASA), as part of the *XMM–Newton* Survey Science Centre Guaranteed Time programme. The work also made use of archival material from the SIMBAD and VIZIER systems at CDS, Strasbourg, NASA's Astrophysics Data System, the *ROSAT* Data Archive of the Max-Planck-Institut für extraterrestrische Physik (MPE) at Garching, Germany, and the Leicester Data base and Archive Service (LEDAS).

REFERENCES

Arnaud K. A., 1996, in Jacoby G. H., Barnes J., eds, ASP Conf. Ser. Vol. 101, Astronomical Data Analysis Software and Systems V. Astron. Soc. Pac., San Francisco, p. 67
Baraffe I., Chabrier G., Allard F., Hauschildt P. H., 1998, A&A, 337, 403
Berger E., 2002, ApJ, 572, 503
Berger E. et al., 2001, Nat, 410, 338
Boese F. G., 2000, A&AS, 141, 507
Briggs K. R., Pye J. P., 2003a, MNRAS, 345, 714
Briggs K. R., Pye J. P., 2003b, Adv. Space Res., 32, 1081
Delfosse X., Forveille T., Perrier C., Mayor M., 1998, A&A, 331, 581
Feigelson E. D., Broos P., Gaffney J. A., Garmire G., Hillenbrand L. A., Pravdo S. H., Townsley L., Tsuboi Y., 2002, ApJ, 574, 258
Festin L., 1998, MNRAS, 298, L34
Flaccomio E., Micela G., Sciortino S., 2003, A&A, 397, 611
Fleming T. A., 1988, PhD thesis, Univ. Arizona
Fleming T. A., Giampapa M. S., Schmitt J. H. M. M., Bookbinder J. A., 1993, ApJ, 410, 387
Fleming T. A., Giampapa M. S., Schmitt J. H. M. M., 2000, ApJ, 533, 372
Fleming T. A., Giampapa M. S., Garza D., 2003, ApJ, 594, 982
Ghizzardi S., 2002, Technical document, EPIC-MCT-TN-012
Giampapa M. S., Rosner R., Kashyap V., Fleming T. A., Schmitt J. H. M. M., Bookbinder J. A., 1996, ApJ, 463, 707
Gizis J. E., Monet D. G., Reid I. N., Kirkpatrick J. D., Liebert J., Williams R. J., 2000, AJ, 120, 1085
Güdel M., Audard M., Reale F., Skinner S. L., Linsky J. L., 2004, A&A, 416, 713
Hambaryan V., Staude A., Schwope A. D., Scholz R.-D., Kimeswenger S., Neuhäuser R., 2004, A&A, 415, 265
Hawley S. L., Johns-Krull C. M., 2003, ApJ, 588, L109
Hodgkin S. T., Jameson R. F., Steele I. A., 1995, MNRAS, 274, 869
Imanishi K., Tsujimoto M., Koyama K., 2001, ApJ, 563, 361
Jayawardhana R., Mohanty S., Basri G., 2003, ApJ, 592, 282
Kraft R. P., Burrows D. N., Nousek J. A., 1991, ApJ, 374, 344
Liebert J., Kirkpatrick J. D., Cruz K. L., Reid I. N., Burgasser A., Tinney C. G., Gizis J. E., 2003, AJ, 125, 343
Martín E. L., 1999, MNRAS, 302, 59
Martín E. L., Ardila D. R., 2001, AJ, 121, 2758
Martín E. L., Basri G., Zapatero Osorio M. R., Rebolo R., López R. J. G., 1998, ApJ, 507, L41 (M98)
Martín E. L., Brandner W., Bouvier J., Luhman K. L., Stauffer J., Basri G., Zapatero Osorio M. R., Barrado y Navascués D., 2000, ApJ, 543, 299
Meyer F., Meyer-Hofmeister E., 1999, A&A, 341, L23
Mohanty S., Basri G., 2003, ApJ, 583, 451
Mohanty S., Basri G., Shu F., Allard F., Chabrier G., 2002, ApJ, 571, 469
Mokler F., Stelzer B., 2002, A&A, 391, 1025
Neuhäuser R., Comerón F., 1998, Sci, 282, 83
Neuhäuser R. et al., 1999, A&A, 343, 883 (N99)
Neuhäuser R., Guenther E. W., Petr M. G., Brandner W., Huélamo N., Alves J., 2000, A&A, 360, L39
Orlando S., Peres G., Reale F., 2000, ApJ, 528, 524
Pan X., Shao M., Kulkarni S. R., 2004, Nat, 427, 326
Paresce F., 1984, AJ, 89, 1022
Pinfield D. J., Hodgkin S. T., Jameson R. F., Cossburn M. R., Hambly N. C., Devereux N., 2000, MNRAS, 313, 347
Pinfield D. J., Dobbie P. D., Jameson R. F., Steele I. A., Jones H. R. A., Katsiyannis A. C., 2003, MNRAS, 342, 1241
Preibisch T., Zinnecker H., 2002, AJ, 123, 1613
Reale F., Peres G., Orlando S., 2001, ApJ, 557, 906
Rebolo R., Zapatero Osorio M. R., Martín E. L., 1995, Nat, 377, 129 (R95)
Rebolo R., Martín E. L., Basri G., Marcy G. W., Zapatero Osorio M. R., 1996, ApJ, 469, L53
Reid N., Hawley S. L., Mateo M., 1995, MNRAS, 272, 828
Rutledge R. E., Basri G., Martín E. L., Bildsten L., 2000, ApJ, 538, L141
Schmitt J. H. M. M., Liefke C., 2002, A&A, 382, L9
Schmitt J. H. M. M., Fleming T. A., Giampapa M. S., 1995, ApJ, 450, 392
Smith R. K., Brickhouse N. S., Liedahl D. A., Raymond J. C., 2001, ApJ, 556, L91
Stauffer J. R., 1984, ApJ, 280, 189
Stauffer J. R., Schultz, G., Kirkpatrick J. D., 1998, ApJ, 499, L199
Strüder L. et al., 2001, A&A, 365, L18
Tinney C. G., 1998, MNRAS, 296, L42
Tinney C. G., Reid I. N., 1998, MNRAS, 301, 1031
Tsuboi Y., Maeda Y., Feigelson E. D., Garmire G. P., Chartas G., Mori K., Pravdo S. H., 2003, ApJ, 587, L51
Turner M. J. L. et al., 2001, A&A, 365, L27
Zapatero Osorio M. R., Rebolo R., Martín E. L., 1997a, A&A, 317, 164
Zapatero Osorio M. R., Rebolo R., Martín E. L., Basri G., Magazzu A., Hodgkin S. T., Jameson R. F., Cossburn M. R., 1997b, ApJ, 491, L81 (Z97)
Zapatero Osorio M. R., Rebolo R., Martín E. L., Hodgkin S. T., Cossburn M. R., Magazzù A., Steele I. A., Jameson R. F., 1999, A&AS, 134, 537 (Z99)

This paper has been typeset from a TEX/LATEX file prepared by the author.